Observed Relationships between the El Niño–Southern Oscillation and the Extratropical Zonal-Mean Circulation

MICHELLE L. L'HEUREUX* AND DAVID W. J. THOMPSON

Department of Atmospheric Science, Colorado State University, Fort Collins, Colorado

(Manuscript received 10 February 2005, in final form 27 July 2005)

ABSTRACT

There is increasing evidence indicating that the climate response to variations in the El Niño–Southern Oscillation (ENSO) includes not only thermally forced zonal wind anomalies in the subtropics but also eddy-driven zonal wind anomalies that extend into the mid–high latitudes of both hemispheres. In this study, new insights into the observed seasonally varying signature of ENSO in the extratropical zonal-mean circulation are provided and the associated linkages with the dominant patterns of extratropical variability are examined.

The zonal-mean extratropical atmospheric response to ENSO is characterized by two principal features: an equivalent barotropic dipole in the Southern Hemisphere (SH) zonal-mean zonal flow with centers of action located near ~40° and ~60° during austral summer, and a weaker, but analogous, dipole in the Northern Hemisphere (NH) with centers of action located near ~25° and ~45° during early and late boreal winter. Both structures are accompanied by eddy momentum flux anomalies that exhibit a remarkable degree of hemispheric symmetry. In the SH, the extratropical signature of ENSO projects strongly onto the primary mode of large-scale variability, the southern annular mode (SAM). During the austral summer, roughly 25% of the temporal variability in the SAM is linearly related to fluctuations in the ENSO cycle. An analogous relationship is not observed in association with the principal mode of climate variability in the NH, the northern annular mode (NAM).

It is argued that the seasonally varying impact of ENSO on the extratropical circulation is consistent with the impact of the thermally forced subtropical wind anomalies on the dissipation of equatorward-propagating wave activity at subtropical latitudes.

1. Introduction

The El Niño–Southern Oscillation (ENSO) has a widely established impact on the zonally symmetric circulation at tropical latitudes and the zonally asymmetric circulation at extratropical latitudes. At tropical latitudes, ENSO is characterized by zonal-mean temperature anomalies that reflect the tropical tropospheric response to anomalous convection in the Pacific sector (e.g., Yulaeva and Wallace 1994). The tropical temperature anomalies, in turn, give rise to zonally symmetric anomalies in the subtropical zonal flow of both hemispheres, consistent with thermal wind balance (e.g., Arkin 1982). In the extratropics, ENSO is associated with zonally asymmetric wave-like anomalies extending from subtropical latitudes to the mid- to high latitudes of both hemispheres (Horel and Wallace 1981; Mo and White 1985; Karoly 1989; Trenberth et al. 1998; Garreaud and Battisti 1999). The zonally asymmetric extratropical signature of ENSO is indicative of the generation of Rossby waves by anomalous vorticity advection in the deep Tropics (Hoskins and Karoly 1981; Sardeshmukh and Hoskins 1988).

There is increasing interest in the observed impact of ENSO on the zonal-mean circulation in the extratropics. For example, Karoly (1989) demonstrates that ENSO is associated with a dipole in the zonal-mean zonal wind in the extratropics of the Southern Hemisphere (SH) during austral summer [December–January–February (DJF)] but not during austral winter [June–July–August (JJA)]. Robinson (2002) reveals ENSO is marked by zonally symmetric tropospheric

* Current affiliation: NOAA/NWS/NCEP/Climate Prediction Center, Camp Springs, Maryland.

Corresponding author address: Michelle L'Heureux, NOAA/NWS/NCEP/Climate Prediction Center, Rm. 605, 5200 Auth Rd., Camp Springs, MD 20746.
E-mail: michelle.lheureux@noaa.gov

temperature anomalies centered around ~30°–40°N during boreal summer. Seager et al. (2003) note the leading empirical orthogonal function (EOF) of global 300-hPa zonal wind anomalies, which describes out-of-phase fluctuations between the strength of the subtropical jets and the mid–high-latitude zonal flow in both hemispheres, is closely related to variations in ENSO. Seager et al. (2003) go on to argue that the observed relationships between ENSO and the extratropical zonal flow are consistent with the impact of changes in the index of refraction on the propagation of transient eddies.

The relationships between ENSO and the extratropical zonal-mean zonal flow are important not only because of ENSO's impact on the midlatitude circulation but also because of possible interactions between ENSO and the principal modes of extratropical variability, the annular modes. The northern annular mode (NAM) and southern annular mode (SAM) describe nearly zonally symmetric vacillations in the extratropical zonal flow of their respective hemispheres (e.g., Thompson and Wallace 2000). The equivalent barotropic structure of these patterns reflects the fact they are both driven by anomalies in the eddy flux of zonal momentum at midlatitudes: during the so-called high index polarity of the annular modes, the anomalous poleward flux of eddy momentum across ~45°–50° latitude drives westerly anomalies at ~55°–60° and easterly anomalies at ~35°–40°, and vice versa (e.g., Karoly 1990; Hartmann and Lo 1998; Thompson and Wallace 2000; Limpasuvan and Hartmann 2000; Lorenz and Hartmann 2001, 2003).

The internal dynamics of the annular modes have been widely investigated, but less investigated is the relationship between these structures and ENSO. Quadrelli and Wallace (2002) demonstrate that the structure of the NAM is significantly different during opposing phases of the ENSO cycle, but find no analogous relationship with the SAM. Ribera and Mann (2003) follow the evolution of a 3–6-yr ENSO signal from peak warm to cold events and observe that the signal is significantly correlated (90° out of phase) with the SAM. Carvalho et al. (2005) use composites to show that the negative polarity of the SAM emerges when warm, low-frequency SSTs are observed over the central-eastern Pacific, as is the case during the warm phase of ENSO.

The purpose of this contribution is to document aspects of the seasonally varying signature of ENSO in the zonal-mean extratropical circulation that are not highlighted in the previous literature and to examine the seasonally varying linear relationships between ENSO and the annular modes of variability. The results draw from findings first reported in L'Heureux (2004). As noted in Robinson (2002) and Seager et al. (2003), it is shown that ENSO has a significant impact on the zonally symmetric extratropical circulation, and that this impact exhibits a remarkable degree of hemispheric symmetry. However, in contrast to previous studies, we also show the following: 1) the impact of ENSO on the extratropical zonal-mean flow exhibits a distinct seasonality, 2) the meridional structure of the zonal-mean response to ENSO differs between the two hemispheres in a manner consistent with the respective background climatologies, and 3) ENSO explains ~25% of the temporal variability in the SAM during austral summer but is not significantly correlated with the NAM during any season. It is further argued that the extratropical signature of ENSO at least partially reflects the impact of the thermally forced ENSO wind anomalies on the dissipation of wave activity at subtropical latitudes.

The paper is outlined as follows. In section 2, we discuss the analysis procedure and data. Section 3 examines the seasonally varying signature of ENSO in the zonal-mean zonal wind as a function of latitude. We reveal ENSO is associated with two principal features in the extratropical zonal-mean flow: a dipole in the zonal-mean zonal wind located around ~60° and ~40° latitude in the SH during austral summer, and ~25° and ~45° latitude in the Northern Hemisphere (NH) during both early and late boreal winter. In sections 4 and 5, we explore the SH and NH features in greater detail and provide a partial interpretation of the results. Section 6 summarizes the major findings.

2. Data and methodology

The primary data used in this research are monthly mean values of the National Centers for Environmental Prediction–National Center for Atmospheric Research (NCEP–NCAR) reanalysis, which includes an extensive archive of observational data assimilated using a state-of-the-art forecast model (Kalnay et al. 1996; Kistler et al. 2001). The data were obtained from the National Oceanic and Atmospheric Administration (NOAA) Climate Diagnostic Center (CDC) and are gridded on a 2.5° × 2.5° mesh. Because of concerns with data quality prior to the incorporation of global satellite soundings, particularly in the SH, we restrict our analysis to the 26 yr following 1978 (May 1979–March 2004). We also briefly make use of model data from the National Aeronautics and Space Administration (NASA) Seasonal-to-Interannual Prediction Proj-

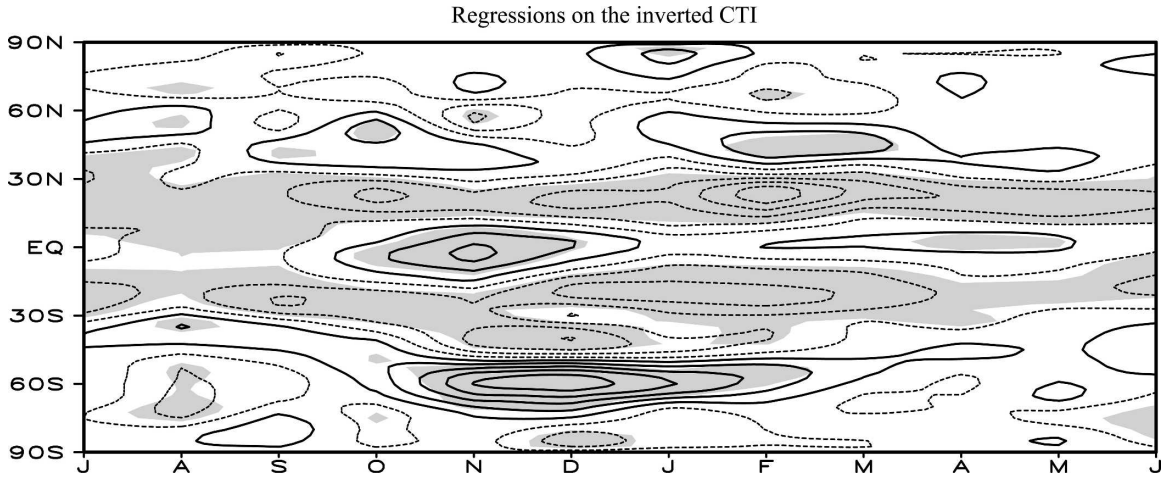

FIG. 1. Monthly mean 300-hPa zonal-mean zonal wind anomalies regressed onto inverted values of the CTI time series for January 1979–December 2003. Results are plotted as a function of month (ordinate) and latitude (abscissa). Values of the CTI have been standardized and detrended. Contour interval is 0.5 m s^{-1} (−0.75, −0.25, 0.25). Shading denotes relationships at the 95% significance level based on a one-tailed test of the *t* statistic.

ect Atmospheric General Circulation Model (NSIPP AGCM; Bacmeister et al. 2000). The model results are derived from simulations in which the AGCM is run for 20 yr with seasonally varying prescribed sea surface temperatures (SSTs) corresponding to perpetual El Niño and La Niña conditions, respectively. The prescribed SST anomalies were found by calculating the leading EOFs of global SST anomalies and then superposing the ENSO-like leading EOF pattern on top of the seasonally varying climatological mean SSTs (see the Web site nsipp.gsfc.nasa.gov for details). The amplitude of the ENSO-like EOF corresponds to an ENSO event that is two standard deviations about the climatology. Hence, the model results are divided by two to facilitate comparison with the observations.

Monthly time series of the NAM and the SAM were obtained from the NOAA Climate Prediction Center Web site (www.cpc.ncep.noaa.gov). The SAM (NAM) index is defined as the first principal component of monthly 700-hPa (1000-hPa) geopotential height anomalies from the NCEP–NCAR reanalysis dataset. Variations in ENSO are defined on the basis of SST anomalies averaged over a region spanning 6°N–6°S, 180°–90°W. The so-called cold tongue index (CTI) is available online from the Joint Institute for the Study of the Atmosphere and Ocean (JISAO) at the University of Washington (tao.atmos.washington.edu/data_sets/). All indices were standardized and detrended prior to all analyses.

In some cases, we decompose the spatial signature of ENSO into fractions linearly congruent with and linearly independent of the spatial structure of the SAM. For example, the component of structure function $A(x)$ that is linearly congruent with $B(x)$ is given as $\alpha \cdot B(x)$, where α is the regression coefficient found by regressing $A(x)$ onto $B(x)$. Hence, the component of a spatial pattern that is linearly congruent with the structure of the SAM in the month-to-month variability is found by 1) regressing the spatial pattern onto the corresponding SAM regression map and 2) then multiplying the SAM regression map by the resulting spatial regression coefficient. The fitting methodology reveals the amplitude and structure of that component of the spatial pattern that is linearly related to the spatial structure of the SAM. In all cases, statistical significance is evaluated using a one-tailed test of the *t* statistic.

3. The seasonally varying signature of ENSO in the extratropical zonal-mean circulation

Figure 1 shows monthly mean, 300-hPa, zonal-mean zonal wind anomalies regressed onto standardized and detrended values of the inverted CTI time series as a function of month and latitude. Since the CTI is inverted, the zonal wind anomalies in Fig. 1 (and in subsequent figures) correspond to the cold phase of the ENSO cycle; the warm phase is represented by anomalies of the opposite sign.

Immediately evident in Fig. 1 are the statistically significant easterly anomalies that span the subtropical latitudes of both hemispheres throughout the year. As shown in previous studies (e.g., Arkin 1982; Yulaeva and Wallace 1994), the subtropical easterly anomalies are attributable to anomalous cooling in the Tropics, which leads to a decrease in the equator-to-pole temperature gradient and, consistent with thermal wind

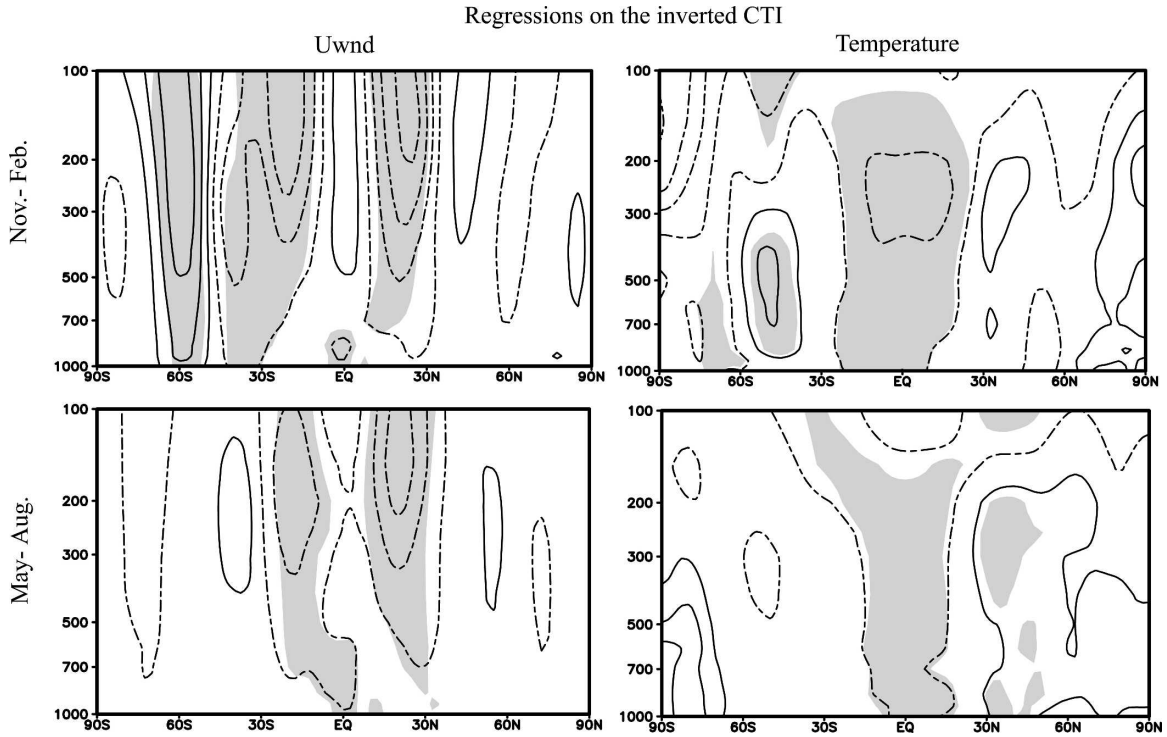

FIG. 2. (top left) Monthly mean zonal mean zonal wind anomalies regressed onto inverted values of the CTI time series for November–February. (top right) As in the left panel but for zonal-mean temperature anomalies. (bottom) As in the top panels but for May–August. Contour intervals are 0.5 m s^{-1} (−0.75, −0.25, 0.25) and 0.2 K (−0.30, −0.10, 0.10). Results are based on the period from May 1979 to February 2004. Shading denotes relationships at the 95% significance level based on a one-tailed test of the *t* statistic.

balance, reduced westerly vertical shear at subtropical latitudes.

The subtropical zonal wind anomalies revealed in Fig. 1 are widely established in the literature, but the figure also captures three robust anomalies beyond those expected due to anomalous tropical heating. First, anomalous westerlies are evident near the equator between October and December and, to a lesser extent, April. Second, the zonal flow in the NH is marked by a meridional dipole in zonal wind anomalies with anomalous westerlies near ~45°N and enhanced subtropical easterly anomalies near ~25°N during early and late boreal winter but less so during boreal midwinter. And third, an analogous meridional dipole is apparent in the SH but with westerly anomalies at ~60°S accompanied by easterly anomalies at ~40°S latitude during the austral summer.

The extratropical structures revealed in Fig. 1 are statistically significant at the 95% level, and the key aspects of their seasonality are recovered in the first and second halves of the data. In the following sections, we explore the details of these features in greater detail. Section 4 focuses on the anomalies in the SH during austral summer; section 5 on the anomalies in the NH during early and late boreal winter.

4. The signature of ENSO in the Southern Hemisphere zonal-mean circulation

To further explore the SH extratropical anomalies revealed in Fig. 1, we subdivide the analyses into the austral summer (November–February) and austral winter (May–August) seasons. Figure 2 shows the regression of zonal-mean zonal wind (left panels) and temperature (right panels) anomalies onto inverted values of the CTI at all levels in the troposphere. During both seasons, the subtropical easterly anomalies linked to ENSO are nearly symmetric about the equator and have largest amplitude in the upper troposphere with little amplitude near the surface (Fig. 2, left panels). As noted above, the subtropical easterly wind anomalies are consistent with diabatic cooling of the tropical troposphere (Fig. 2, right panels) and do not have a strong barotropic component. The subtropical zonal wind anomalies are somewhat weaker during the austral winter, presumably because variations in tropical heating associated with ENSO are reduced at this time.

The most remarkable feature in Fig. 2 is the meridional dipole in zonal–wind anomalies in the mid–high-latitude SH during the austral summer (top-left panel). In contrast to the zonal wind anomalies at subtropical

latitudes, the westerly anomalies at ~60°S and easterly anomalies at ~40°S extend through the depth of the troposphere and have substantial amplitude at the surface. A similar zonal wind feature is observed in Karoly (1989). As noted in Seager et al. (2003), the dipole in zonal wind anomalies is accompanied by warming at midlatitudes centered at ~50°S (Fig. 2, top-right panel).

The SH zonal wind anomalies in the top-left panel of Fig. 2 bear strong resemblance to the structure of the SAM; both ENSO and the SAM are associated with equivalent barotropic, zonally symmetric zonal wind anomalies in the extratropics of the SH. As discussed in section 2, the apparent similarity between the climate response to ENSO and the SAM can be quantified by linearly fitting the spatial structure of the SAM to regression maps based on the CTI time series. The regression map in the top-left panel of Fig. 2 (reproduced in the top panel of Fig. 3) is thus partitioned into a component that is linearly congruent with the structure of the SAM in the month-to-month variability (the "SAM fit"; middle panel of Fig. 3) and a component that is linearly independent of the structure of the SAM (the "SAM residual"; bottom panel of Fig. 3). As evidenced in Fig. 3, the SAM fit accounts for virtually all of the structure and amplitude of the response of the SH zonal-mean circulation to variations in the ENSO cycle. The component of the ENSO signature that is linearly independent of the SAM (Fig. 3, bottom panel) bears close resemblance to the pattern expected solely due to variations in tropical heating, and is reminiscent of the signature of ENSO in the zonal-mean circulation during the austral winter season (cf. Fig. 3, bottom panel, with Fig. 2, bottom-left panel).

The SAM accounts for a considerable fraction of the SH atmospheric response to ENSO not only in the zonal-mean circulation but in the zonally varying circulation as well. Figure 4a shows monthly mean 500-hPa geopotential height anomalies during November–February regressed onto inverted values of the CTI. As noted in previous studies (e.g., Mo and White 1985; Karoly 1989; Mo 2000; Mo and Nogués-Paegle 2001), ENSO is associated with substantial wavelike anomalies in the SH 500-hPa geopotential height field, with opposing centers of action located to the southeast of New Zealand, to the east of the Ross Sea near coastal Antarctica, and to the southwest of South Africa. As evidenced in Fig. 4a, ENSO is also associated with pronounced zonally symmetric SH geopotential height anomalies, such that the cold phase of ENSO is distinguished by lower than normal geopotential height anomalies throughout the SH polar regions but higher than normal height anomalies at middle latitudes. Figure 4b shows the components of the ENSO-related geo-

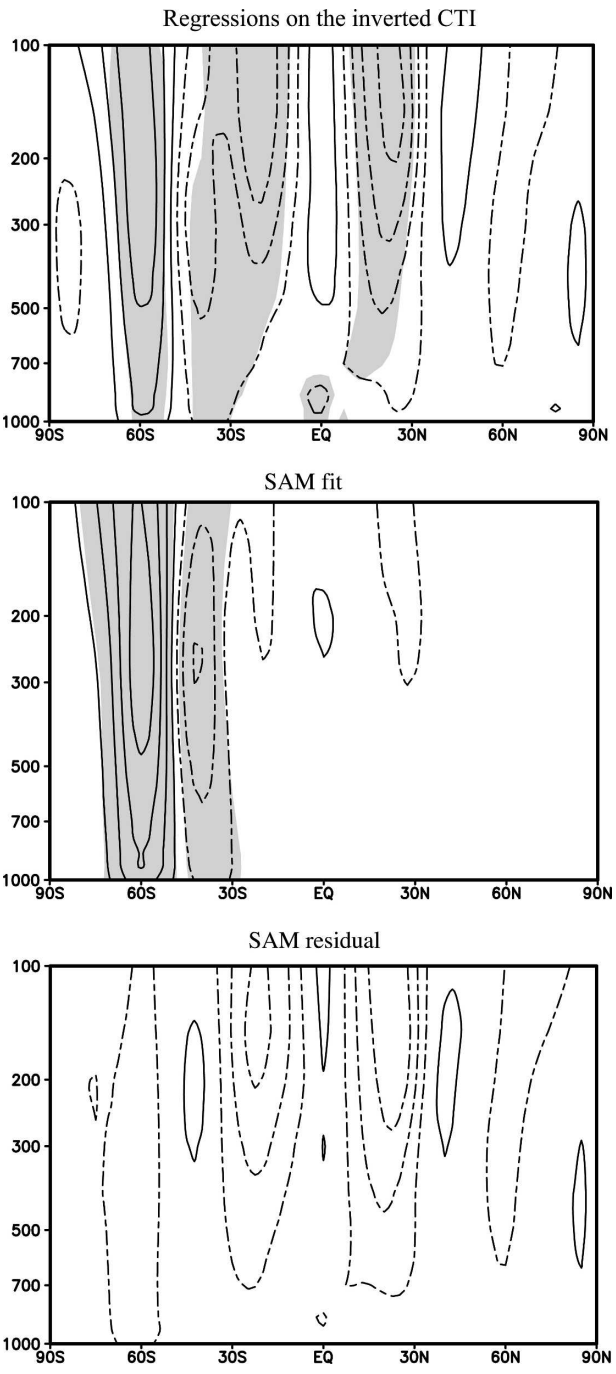

FIG. 3. (top) Repeated from Fig. 2, top left. (middle) The component of the ENSO regression map that is linearly congruent with the structure of the SAM in the month-to-month variability. (bottom) The residual found by subtracting the middle panel from the top panel. Contour interval is 0.5 m s^{-1} (−0.75, −0.25, 0.25). Shading denotes relationships at the 95% significance level based on a one-tailed test of the *t* statistic.

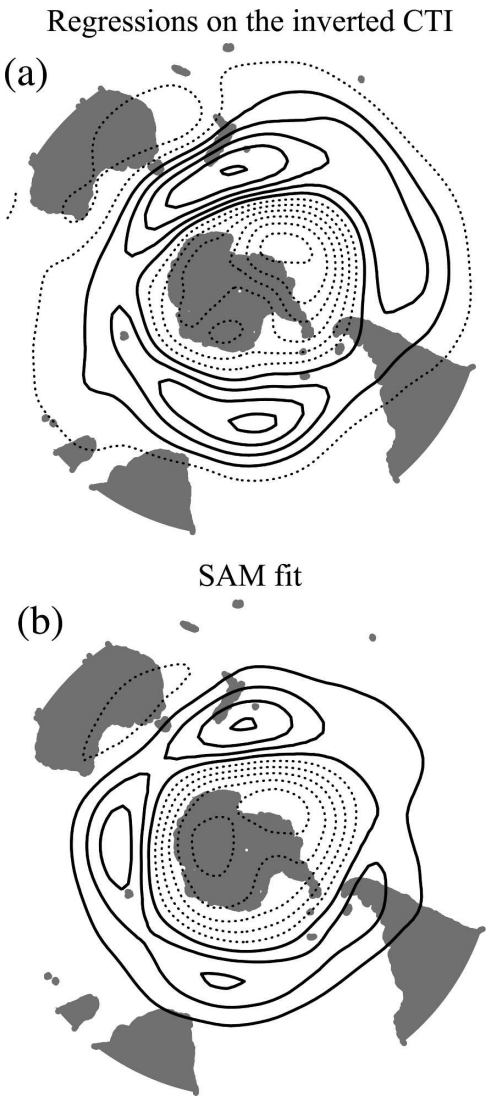

FIG. 4. (top) Monthly mean November–February 500-hPa geopotential height anomalies regressed onto inverted values of the CTI time series. (bottom) The component of the ENSO regression map that is linearly congruent with the structure of the SAM in the month-to-month variability. Contour interval is 5 m (−7.5, −2.5, 2.5).

potential height anomalies that are linearly congruent with the SAM. The results reveal that nearly all of the zonal symmetric component of the ENSO regression map projects onto the structure of the SAM.

As implied by the results in Figs. 1–4, time series of ENSO and the SAM are significantly correlated during the austral summer season (Fig. 5). The contemporaneous correlation coefficient between November–February means of the CTI and SAM index time series is −0.52, which exceeds the 99% confidence level based on a one-tailed test of the *t* statistic. Thus, ~25% of the interannual variance in the SAM during the austral summer season is described by temporal variability in the ENSO cycle. Most of the largest warm ENSO events, including those that occurred during the 1982/83, 1991/92, and 1997/98 seasons, are mirrored by dips in the SAM index.

What drives the SH extratropical zonal-mean response to ENSO? The key processes that drive variations in the SAM can be inferred from the quasigeostrophic zonal-mean form of the zonal momentum equation (e.g., Holton 2004). In this case, changes in the upper-tropospheric zonal-mean zonal wind are primarily driven by the Coriolis force acting on the mean meridional circulation ($f_o[v]$) or the meridional convergence of the eddy momentum flux ($-(\partial[u^*v^*]/\partial y)$). Figure 6 shows monthly mean values of $f_o[v]$ (left panel, solid), $-\partial[u^*v^*]/\partial y$ (right panel, solid), and $[u]$ (both panels, dashed lines) at 300 hPa regressed onto November–February values of the inverted CTI time series. Consistent with results presented in Seager et al. (2003), the Coriolis force acting on the mean meridional circulation anomalies opposes the signature of ENSO in the SH upper-tropospheric zonal-mean zonal flow, whereas the convergence of the eddy momentum flux anomalies reinforces the zonal wind anomalies at both ~40° and ~60°S [Fig. 6, right panel; note the eddy momentum flux anomalies are cosine weighted as in Edmon et al. (1980)]. Hence, the signature of ENSO in the extratropical SH zonal-mean circulation is driven by variations in the eddy momentum flux at middle latitudes.

The relationship between ENSO and the eddy momentum flux is explored further in Fig. 7. The top panel in Fig. 7 shows November–February values of the anomalous eddy momentum flux regressed onto inverted values of the CTI (solid line) and SAM index (dashed line) time series. In the SH midlatitudes, the ENSO-related eddy momentum flux anomalies correspond closely to those found in conjunction with the SAM; both the cold phase of ENSO and the high index polarity of the SAM are characterized by anomalous southward momentum fluxes centered around ~50°S. However, in the SH subtropics, ENSO is associated with substantial northward eddy momentum flux anomalies between ~35° and ~10°S that are not shared by variations in the SAM. Hence, at subtropical latitudes the cold phase of ENSO is linked to both weaker than normal zonal wind anomalies (Fig. 6, dashed line) and anomalous northward eddy momentum fluxes (Fig. 7, top panel). The associated anomalous eddy momentum flux convergence between ~5° and ~25°S acts to dampen, not drive, the easterly zonal wind anomalies in the SH subtropics (Fig. 6, right panel).

Seager et al. (2003) have suggested ENSO-related

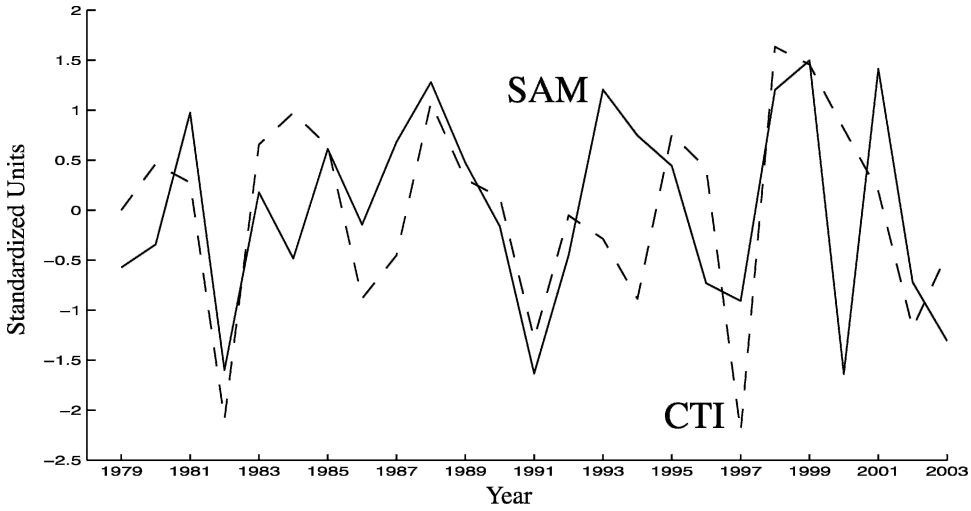

FIG. 5. November–February seasonal mean values of the SAM index time series (solid) and the inverted CTI time series (dashed). Years on the ordinate represent November and December of the season being averaged. Values of the CTI and SAM index are standardized and detrended. The correlation coefficient between the CTI and SAM is −0.52.

variations in the strength of the subtropical zonal flow act to refract transient extratropical eddies in the meridional plane, thus driving the pattern of eddy momentum fluxes observed in the top panel of Fig. 7. An alternative interpretation motivated by Figs. 6 and 7 is that changes in the strength of the subtropical zonal flow associated with ENSO impact the meridional group velocity of equatorward-propagating eddies and thus the latitude of maximum eddy dissipation. For example, the meridional group velocity for low-frequency Rossby waves decreases as the strength of the zonal wind diminishes (e.g., Hoskins and Karoly 1981; Webster and Holton 1982). In the climatological mean, wave activity is primarily directed from middle to subtropical latitudes in the upper troposphere (Fig. 7, bottom panel; note the flux of wave activity is directed opposite the eddy momentum flux). Therefore, during the cold phase of the ENSO cycle, waves propagating equatorward in the upper troposphere experience weaker than normal background flow, have lower than normal meridional group velocities, and thus will tend to dissipate at anomalously poleward locations. In this case, the anomalous flux of wave activity will be directed southward in the SH subtropics, with decreased wave drag in the deep SH subtropics and increased wave drag on the poleward flank of the subtropics.

The above hypothesis is consistent with the anomalous southward flux of wave activity near ~30°S (Fig. 7,

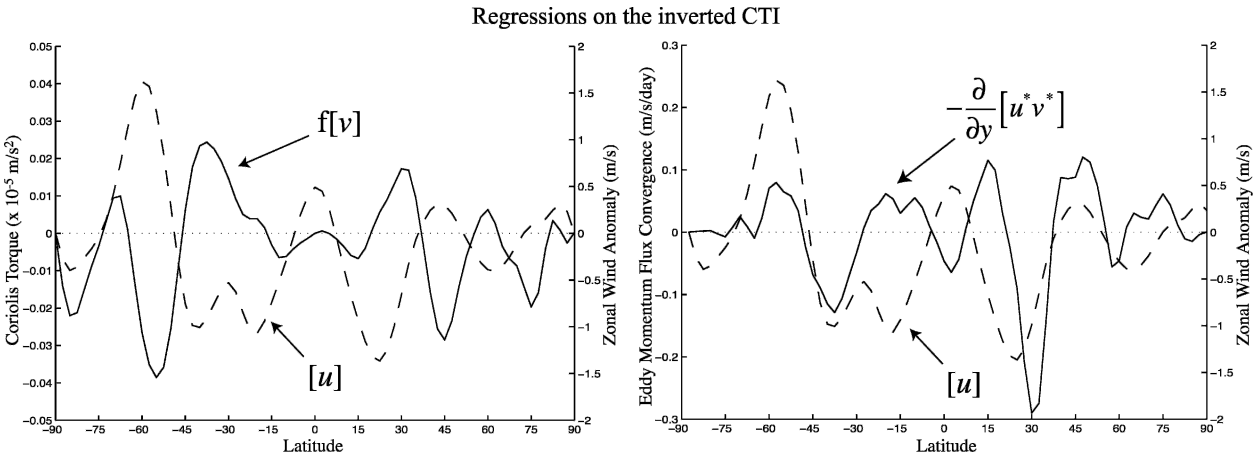

FIG. 6. (left) Monthly mean 300-hPa zonal-mean Coriolis torque anomalies (solid) and zonal-mean zonal wind anomalies (dashed) regressed onto inverted values of the CTI time series for November−February. (right) As in the left panel except the solid line denotes the regression of the 300-hPa zonal-mean eddy momentum flux convergence anomalies onto inverted values of the CTI.

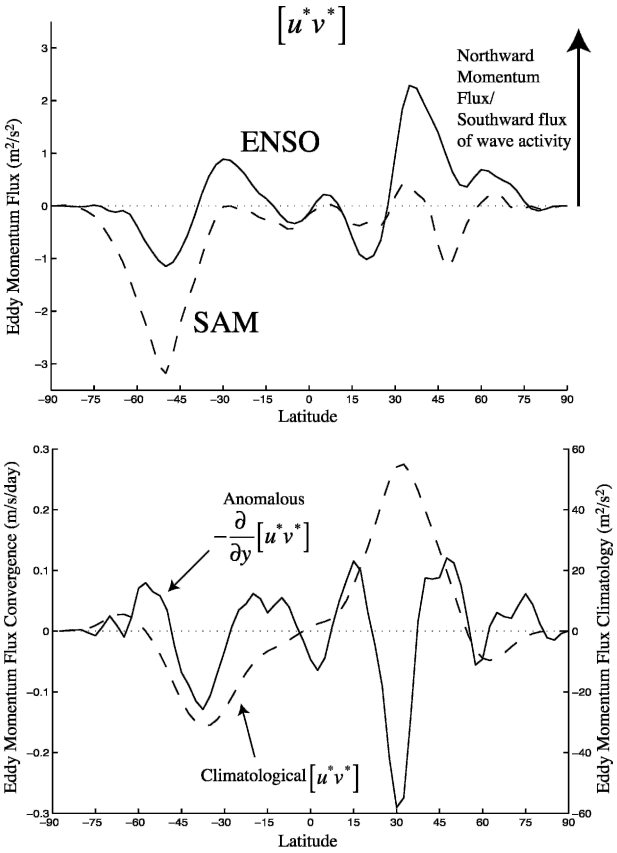

FIG. 7. (top) Monthly mean November–February 300-hPa zonal-mean eddy momentum flux anomalies regressed onto inverted values of the CTI (dashed) and the SAM index (solid) time series. (bottom) The climatological-mean November–February 300-hPa eddy momentum flux (dashed) and eddy momentum flux convergence anomalies regressed onto inverted values of the CTI time series (solid; reproduced from Fig. 6, right panel).

top panel), the anomalous westerly wave forcing around ~20°S, and the anomalous easterly wave forcing near ~40°S (Fig. 6, right; reproduced in Fig. 7, bottom panel). It is also consistent with the fact that the most pronounced ENSO-related wave dissipation anomalies tend to occur in regions where the climatological eddy flux is largest (Fig. 7, bottom panel). However, the above hypothesis does not provide an explanation for the anomalous eddy momentum fluxes ~50°S, which are shared with the SAM (Fig. 7, top panel). One possible explanation for this feature is 1) the anomalous eddy momentum flux divergence near ~40°S drives adiabatic warming at ~50°S (see also Seager et al. 2003), and 2) the associated increases in the meridional temperature gradient poleward of ~50°S shift the region of maximum baroclinic eddy generation poleward in a manner that projects onto the high index polarity of the SAM (e.g., Robinson 2000). To what extent the adiabatic changes in tropospheric temperatures are, in fact, large enough to perturb the growth of baroclinic eddies remains to be determined.

From both Seager et al. (2003) and the results in Figs. 6 and 7, it is apparent that the extratropical response to ENSO exhibits a substantial level of hemispheric symmetry throughout the austral summer/boreal winter months. The NH features in Figs. 6 and 7 primarily reflect the early and late boreal winter anomalies from Fig. 1 and are the focus of the next section.

5. The ENSO signature in the Northern Hemisphere zonal-mean circulation

In this section, we provide a brief companion analysis for the NH zonal-mean zonal wind anomalies evident in Fig. 1 during the early and late boreal winter months. Because the results for the early boreal winter are qualitatively similar to—albeit weaker than—those found in late winter, we only show results for the later winter months of February–March. The season investigated in this section is chosen to highlight the extratropical NH features in Fig. 1, and thus by construction, the month of February is shared with the analyses presented in the previous section.

Figure 8 shows February–March monthly mean zonal-mean zonal wind (left panel) and temperature (right panel) anomalies regressed onto inverted values of the CTI time series for all levels in the troposphere. As expected, the subtropics are distinguished by pronounced easterly zonal wind anomalies in both hemispheres, consistent with Tropics-wide cooling during the cold phase of the ENSO cycle. The NH subtropical zonal wind anomalies at around ~25° are not restricted to the upper troposphere but have significant amplitude near the surface. The results also reveal anomalous westerlies in the extratropics at ~45°N and, as noted in Robinson (2002) and Seager et al. (2003), anomalous warming in the midlatitudes at ~35°N (right panel).

Although not immediately apparent in Fig. 1, a close parallel exists between the dipole in NH zonal wind anomalies located near ~45° and ~25°N during late boreal winter and the dipole in SH zonal wind anomalies located near ~60° and ~40°S during austral summer. As is the case in the SH, the NH zonal wind response is consistent with forcing by anomalous eddy momentum fluxes in the upper troposphere (Fig. 9). Additionally, the largest anomalous NH easterly wave forcing is nearly collocated with the latitude of maximum climatological poleward eddy momentum fluxes (Fig. 10, bottom panel). Hence, the roughly 15° latitudinal shift between the NH and SH extratropical responses to ENSO is also reflected in the climatological-mean eddy momentum fluxes in the two hemispheres.

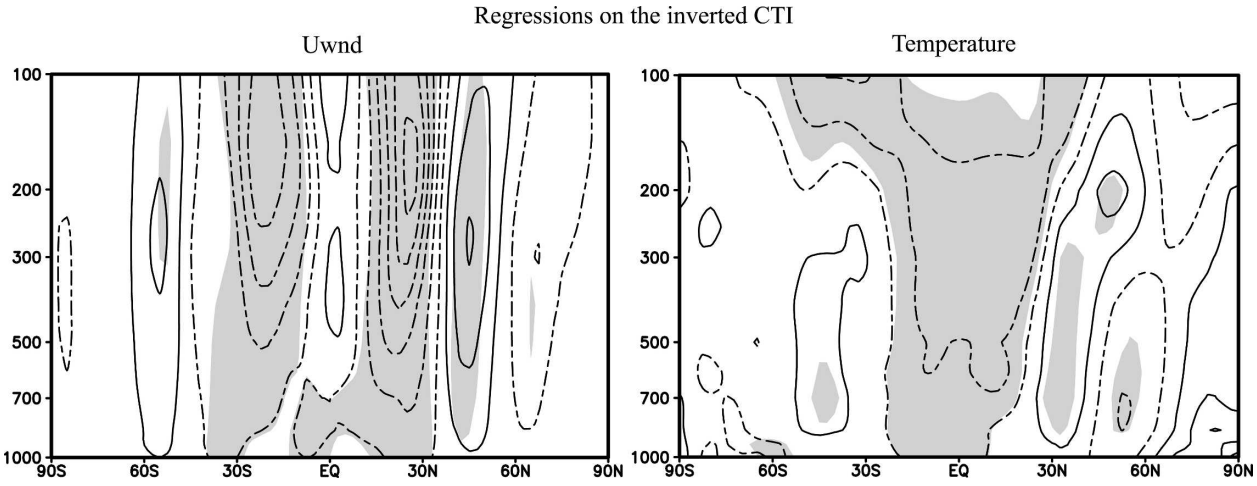

FIG. 8. As in the top panels of Fig. 2 but for monthly mean data during February–March.

In the previous section, we noted the SH eddy momentum flux and zonal wind anomalies linked to ENSO project onto the structure of the SAM during the austral summer. From the top panel in Fig. 10, it is evident an analogous relationship is not observed in association with the NAM. In the NH, the ENSO-related anomalies in the eddy-momentum flux lie ~10° equatorward of the corresponding NAM-related anomalies. Indices of the NAM and ENSO are not significantly correlated during any season (not shown).

6. Discussion

The results in this study confirm ENSO is associated with eddy-driven changes in the extratropical zonal-mean circulation, which exhibit a high degree of hemispheric symmetry. However, the results also highlight three novel aspects of the signature of ENSO in the extratropical zonal-mean zonal flow:

1) The ENSO signature in the zonal-mean extratropical circulation exhibits a distinct seasonality, with the largest anomalies centered during austral summer in the SH but during early and late boreal winter in the NH. In part, the seasonality of the ENSO response is consistent with the observation that the amplitude of the ENSO cycle is largest during the boreal winter/

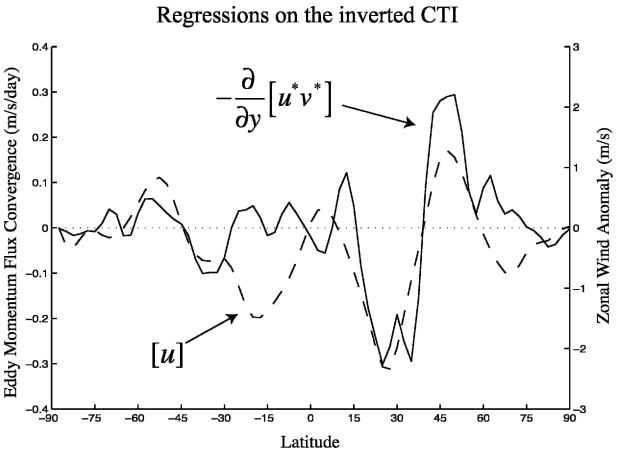

FIG. 9. As in the right panel of Fig. 6 but for regressions based on the NAM index time series during February–March.

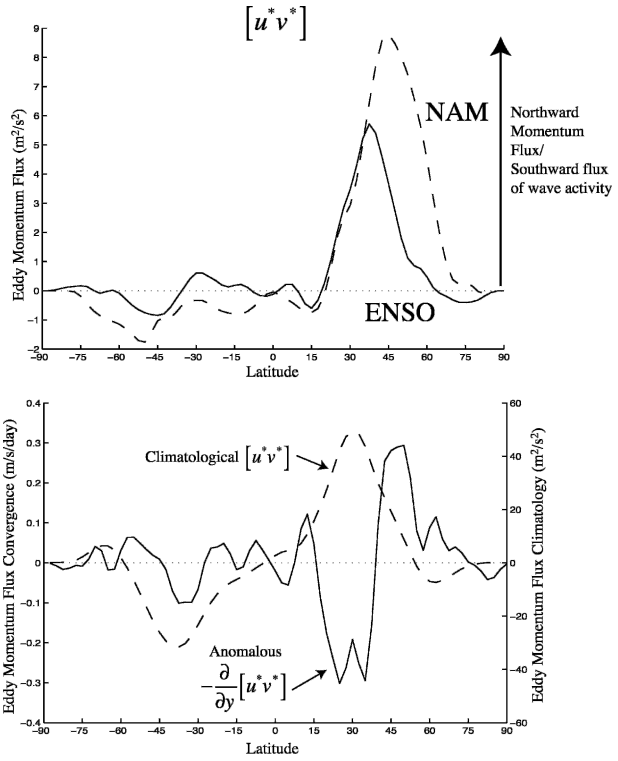

FIG. 10. As in Fig. 7 but for monthly mean data during February–March; the dashed line in the top panel is based on regressions on the NAM index time series.

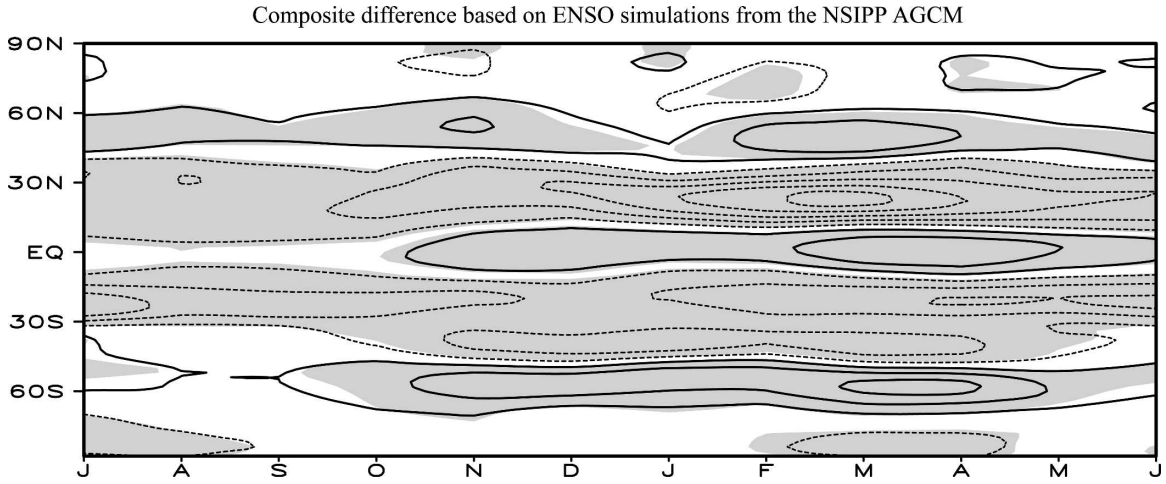

FIG. 11. As in Fig. 1 but for differences between the NSIPP AGCM zonal-mean zonal wind response to prescribed SSTs corresponding to perpetual El Niño and La Niña conditions, respectively. See text for details. Shading denotes differences at the 95% significance level based on a one-tailed test of the *t* statistic.

austral summer (Philander 1990). The dual-maxima in the NH response is reminiscent of the suppression of eddy activity in the North Pacific storm track during the middle of the NH winter season (Nakamura 1992).

2) The SH zonal wind anomalies are centered ~15° poleward of their NH counterparts, with out-of-phase zonal wind anomalies centered near ~40° and ~60° latitude in the SH but near ~25° and ~45° latitude in the NH. Thus, the equatorward component of the dipole in extratropical zonal wind anomalies is distinct from the thermally forced zonal wind anomalies in the subtropics in the SH, but not in the NH. The difference between the meridional structures of the NH and SH response is consistent with the difference in the climatologies of the two hemispheres: in both hemispheres, the cold phase of the ENSO cycle is associated with anomalous easterly forcing (and thus increased wave dissipation) at the latitude of maximum climatological momentum fluxes.

We have argued that the changes in wave dissipation associated with ENSO are consistent with the impact of the subtropical zonal wind anomalies on the group velocity—and hence the rate of dissipation—of equatorward-propagating waves. Our hypothesis is similar, but not identical to, the mechanisms proposed in Robinson (2002) and Seager et al. (2003): Robinson (2002) focuses on the impact of shifts in the critical line on the location of eddy absorption; Seager et al. (2003) emphasize the impact of changes in the zonal-mean flow on the *direction* of wave propagation in the meridional plane; and we stress the relationship between changes in the zonal-mean flow and the *rate* of equatorward wave propagation.

3) Consistent with the interhemispheric differences in the meridional structure of the extratropical response to ENSO, variations in ENSO are significantly correlated with fluctuations in the SAM but not the NAM. During austral summer, ~25% of the year-to-year variability in the SAM is linearly related to fluctuations in ENSO.

The findings reported here exhibit a high degree of statistical significance. The relationship between ENSO and the SAM indices exceeds the 99% confidence level, and the main features of both the NH and SH extratropical responses are evident in both the first and second halves of the data record. Additionally, the principal findings reported in this study are evident in the simulated atmospheric response of the NSIPP AGCM to prescribed SSTs corresponding to the opposing phases of the ENSO cycle (see section 2 for details). Figure 11 is constructed in a manner analogous to Fig. 1 but shows the ensemble mean differences in the NSIPP AGCM zonal-mean zonal wind responses to SSTs that resemble perpetual La Niña and El Niño conditions, respectively. As in the observations, the simulated SH response exhibits centers of action located near ~60° and ~40°S, while the NH response has centers of action located around ~45° and ~25°N. The SH response extends somewhat longer into the calendar year compared to the observations (i.e., into March and April) but nevertheless exhibits maximum amplitude during austral summer. Like the observations, the simulated NH zonal-mean zonal wind anomalies exhibit their largest amplitudes during late boreal winter, with a much weaker secondary maximum also found during early winter. The equivalent barotropic struc-

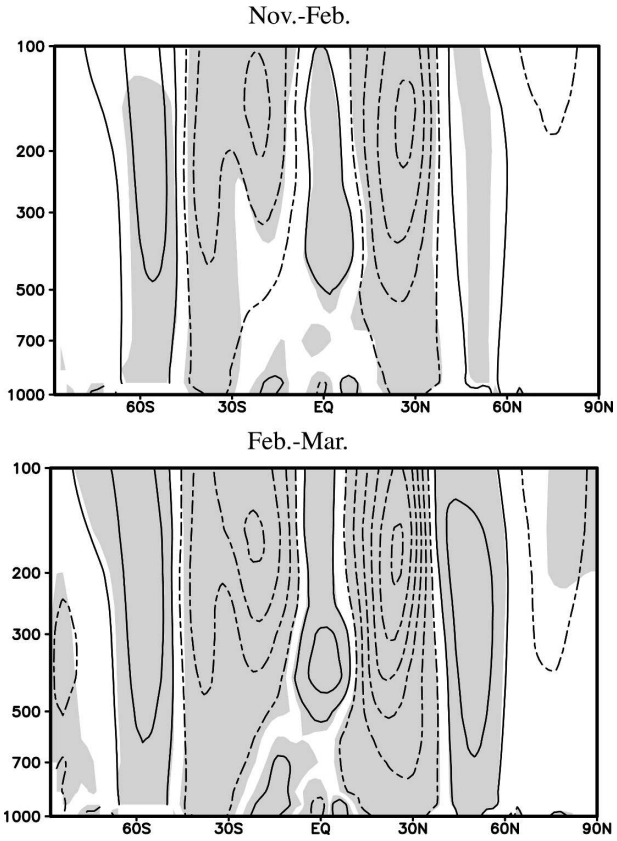

FIG. 12. As in Fig. 2 (top left) and Fig. 8 (left) but for differences between the NSIPP AGCM zonal-mean zonal wind response to prescribed SSTs corresponding to perpetual El Niño and La Niña conditions, respectively. See text for details. Shading denotes differences at the 95% significance level based on a one-tailed test of the *t* statistic.

ture of the extratropical zonal wind anomalies is also readily evident in the simulated differences for the respective austral summer and late boreal winter seasons (Fig. 12).

The results in this study demonstrate a strong linear relationship between two patterns of variability previously thought to be linearly independent: the SAM and ENSO. The results provide an alternative manner through which variations in the ENSO cycle impact climate over the Southern Ocean and also throughout Antarctica.

Acknowledgments. We thank David Randall for valuable discussions and insightful reviews throughout the course of this research. Thanks also to Susan Solomon, Richard Seager, Walter Robinson, and two anonymous reviewers for their helpful comments, and to Siegfried Schubert for assistance with the NSIPP AGCM output. We appreciate the support of R. Wayne Higgins and Jin Huang (GAPP program) during the latter stages of this project. MLL and DWJT were supported under Grants NSF CAREER: ATM-0132190 and NSF ATM-0320959. MLL was also supported under NASA Grant NAG5-11737 and NOAA Cooperative Agreement NA17RJ1228.

REFERENCES

Arkin, P. A., 1982: The relationship between interannual variability in the 200-mb tropical wind field and the Southern Oscillation. *Mon. Wea. Rev.,* **110,** 1393–1404.

Bacmeister, J., P. Pegion, S. Schubert, and M. Suarez, 2000: Atlas of seasonal means simulated by the NSIPP 1 atmospheric GCM. NASA/TM-2000-104505, Tech. Rep. Series on Global Modeling and Data Assimilation, Vol. 17, 1–12.

Carvalho, L. M. V., C. Jones, and T. Ambrizzi, 2005: Opposite phases of the Antarctic Oscillation and relationships with intraseasonal to interannual activity in the Tropics during the austral summer. *J. Climate,* **18,** 702–718.

Edmon, H. J., B. J. Hoskins, and M. E. McIntyre, 1980: Eliassen–Palm cross sections for the troposphere. *J. Atmos. Sci.,* **37,** 2600–2616.

Garreaud, R. D., and D. S. Battisti, 1999: Interannual (ENSO) and interdecadal (ENSO-like) variability in the Southern Hemisphere tropospheric circulation. *J. Climate,* **12,** 2113–2123.

Hartmann, D. L., and F. Lo, 1998: Wave-driven zonal flow vacillation in the Southern Hemisphere. *J. Atmos. Sci.,* **55,** 1303–1315.

Holton, J. R., 2004: *Introduction to Dynamic Meteorology.* Academic Press, 535 pp.

Horel, J. D., and J. M. Wallace, 1981: Planetary-scale atmospheric phenomena associated with the Southern Oscillation. *Mon. Wea. Rev.,* **109,** 813–829.

Hoskins, B. J., and D. J. Karoly, 1981: The steady linear response of a spherical atmosphere to thermal and orographic forcing. *J. Atmos. Sci.,* **38,** 1179–1196.

L'Heureux, M. L., 2004: The observed relationships between the El Niño–Southern Oscillation and the annular modes. M.S. thesis, Deptartment of Atmospheric Science, Colorado State University, 115 pp.

Limpasuvan, V., and D. L. Hartmann, 2000: Wave-maintained annular modes of climate variability. *J. Climate,* **13,** 4414–4429.

Lorenz, D. J., and D. L. Hartmann, 2001: Eddy–zonal flow feedback in the Southern Hemisphere. *J. Atmos. Sci.,* **58,** 3312–3327.

——, and ——, 2003: Eddy–zonal flow feedback in the Northern Hemisphere. *J. Climate,* **15,** 1212–1227.

Kalnay, E., and Coauthors, 1996: The NCEP/NCAR 40-Year Reanalysis Project. *Bull. Amer. Meteor. Soc.,* **77,** 437–471.

Karoly, D. J., 1989: Southern Hemisphere circulation features associated with El Niño–Southern Oscillation events. *J. Climate,* **2,** 1239–1252.

——, 1990: The role of transient eddies in low-frequency zonal variations of the Southern Hemisphere circulation. *Tellus,* **42A,** 41–50.

Kistler, R., and Coauthors, 2001: The NCEP–NCAR 50–year reanalysis: Monthly means CD-ROM and documentation. *Bull. Amer. Meteor. Soc.,* **82,** 247–268.

Mo, K. C., 2000: Relationships between low-frequency variability in the Southern Hemisphere and sea surface temperature anomalies. *J. Climate,* **13,** 3599–3610.

——, and G. H. White, 1985: Teleconnections in the Southern Hemisphere. *Mon. Wea. Rev.,* **113,** 22–37.

——, and J. Nogués-Paegle, 2001: The Pacific–South American modes and their downstream impact. *J. Climatol.,* **21,** 1211–1229.

Nakamura, H., 1992: Midwinter suppression of baroclinic wave activity in the Pacific. *J. Atmos. Sci.,* **49,** 1629–1642.

Philander, S. G., 1990: *El Niño, La Niña, and the Southern Oscillation.* Academic Press, 289 pp.

Quadrelli, R., and J. M. Wallace, 2002: Dependence of the structure of the Northern Hemisphere annular mode on the polarity of ENSO. *Geophys. Res. Lett.,* **29,** 2132, doi:10.1029/2002GL015807.

Ribera, P., and M.E. Mann, 2003: ENSO related variability in the Southern Hemisphere, 1948–2000. *Geophys. Res. Lett.,* **30,** 1006, doi:10.1029/2002GL015818.

Robinson, W. A., 2000: A baroclinic mechanism for the eddy feedback on the zonal index. *J. Atmos. Sci.,* **57,** 415–422.

——, 2002: On the midlatitude thermal response to tropical warmth. *Geophys. Res. Lett.,* **29,** 1190, doi:10.1029/2001GL014158.

Sardeshmukh, P. D., and B. J. Hoskins, 1988: The generation of global rotational flow by steady idealized tropical divergence. *J. Atmos. Sci.,* **45,** 1228–1251.

Seager, R., N. Harnik, Y. Kushnir, W. Robinson, and J. A. Miller, 2003: Mechanisms of hemispherically symmetric climate variability. *J. Climate,* **16,** 2960–2978.

Thompson, D. W. J., and J. M. Wallace, 2000: Annular modes in the extratropical circulation. Part I: Month-to-month variability. *J. Climate,* **13,** 1000–1016.

Trenberth, K. E., G. W. Branstator, D. Karoly, A. Kumar, N. Lau, and C. Ropelewski, 1998: Progress during TOGA in understanding and modeling global teleconnections associated with tropical sea surface temperatures. *J. Geophys. Res.,* **103,** 14 291–14 324.

Webster, P. J., and J. R. Holton, 1982: Cross-equatorial response to middle-latitude forcing with a latitudinally and zonally nonuniform basic state. *J. Atmos. Sci.,* **39,** 722–733.

Yulaeva, E., and J. M. Wallace, 1994: The signature of ENSO in global temperature and precipitation fields derived from the microwave sounding unit. *J. Climate,* **7,** 1719–1736.